Anharmonic effects in the optical and acoustic bending modes of graphene

R. Ramírez,* E. Chacón, and C. P. Herrero

Instituto de Ciencia de Materiales de Madrid (ICMM), Consejo Superior de Investigaciones Científicas (CSIC), Campus de Cantoblanco, 28049 Madrid, Spain

(Received 17 March 2016; revised manuscript received 17 May 2016; published 13 June 2016)

The out-of-plane fluctuations of carbon atoms in a graphene sheet have been studied by means of classical molecular dynamic simulations with an empirical force field as a function of temperature. The Fourier analysis of the out-of-plane fluctuations often applied to characterize the acoustic bending mode of graphene is extended to the optical branch, whose polarization vector is perpendicular to the graphene layer. This observable is inaccessible in a continuous elastic model of graphene but it is readily obtained by the atomistic treatment. Our results suggest that the long-wavelength limit of the acoustic out-of-plane fluctuations of a free layer without stress is qualitatively similar to that predicted by a harmonic model under a tensile stress. This conclusion is a consequence of the anharmonicity of both in-plane and out-of-plane vibrational modes of the lattice. The most striking anharmonic effect is the presence of a linear term, $\omega_A = v_A k$, in the dispersion relation of the acoustic bending band of graphene at long wavelengths ($k \to 0$). This term implies a strong reduction of the amplitude of out-of-plane oscillations in comparison to a flexural mode with a k^2 dependence in the long-wavelength limit. Our simulations show an increase of the sound velocity associated to the bending mode, as well as an increase of its bending constant, κ, as the temperature increases. Moreover, the frequency of the optical bending mode, $\omega_O(\Gamma)$, also increases with the temperature. Our results are in agreement with recent analytical studies of the bending modes of graphene using either perturbation theory or an adiabatic approximation in the framework of continuous layer models.

DOI: 10.1103/PhysRevB.93.235419

I. INTRODUCTION

The crystalline order of a graphene layer has been the focus of interesting experimental investigations. Diffraction experiments by transmission electron microscopy (TEM) reveal that suspended graphene sheets are not perfectly flat: they exhibit intrinsic microscopic ripples. The TEM atomic-resolution images display that the corrugations are static with typical lengths in the range $L = 20$–200 Å and heights between $h = 2$–20 Å [1]. The bending frequencies for wavelengths on the order of 200 Å are estimated to be of order 10^{10} Hz (0.3 cm^{-1}). They are fast for the time scale of electron diffraction experiments. Thus the origin of the out-of-plane corrugation was suggested to be not of thermal nature, but a consequence of adsorbed impurity atoms sitting on random sites [2]. Nevertheless, the exact origin of the static corrugation in graphene is still unclear and probably the stresses at the boundary of graphene during the device fabrication play also an important role [3]. The essential part of anharmonicity in the corrugation behavior of graphene has been stressed in a recent TEM study [4]. The root-mean-square fluctuation of the graphene roughness was estimated as 1.7 Å at 300 K with a lateral scale of about 100 Å. The most striking result of this diffraction experiment, contrary to intuitive expectation, was the *increase* in the average corrugation height with *decreasing* temperature from 300 to 150 K [4].

Atomistic simulations of the intrinsic ripples in graphene have predicted that anharmonic couplings between bending and stretching modes significantly diminish the mean-square height amplitude $\langle h^2 \rangle$ of the out-of-plane thermal fluctuations. The relation of $\langle h^2 \rangle$ to the number of atoms in the layer N has been described as a power-law behavior $N^{1-(\eta/2)}$, where η is the roughness exponent. The harmonic approximation for a typical flexural mode with a quadratic dispersion relation predicts a vanishing exponent ($\eta = 0$) [5]. Note that this value represents a "catastrophic" divergence as the mean-square height fluctuation grows as the area of the sheet, $\langle h^2 \rangle \propto N$. Consideration of anharmonic effects by Nelson and Peliti results in a lower exponent $\eta = 1$, that diminishes the height fluctuations with respect to the harmonic limit [6]. Interestingly, recent computer simulations report anomalous exponents, η, that may vary depending on the employed potential model and on the simulated ensemble (constant stress or strain) in a range from $\eta = 0.67$ to $\eta = 1.1$ [5,7]. It is believed that such anomalous exponents should be universal quantities, therefore the origin for the variability in the roughness exponents reported in computer simulations remains unexplained [3].

Analytical results from continuous models of graphene provide a picture of the intrinsic surface corrugation that differs in some aspects from the power-law behavior described by an anomalous roughness exponent. The study of anharmonic effects by first-order perturbation theory in Ref. [8] shows that the dispersion relation for the acoustic out-of-plane mode in graphene, $\omega_A(k)$, is linear in the long-wavelength limit ($k \to 0$). The relation $\omega_A = v_A k$, characteristic of sound waves at small k, implies a roughness exponent $\eta = 2$. This behavior is not related to an external tension, i.e., the linear term has a finite value even if the stress of the layer vanishes. An adiabatic approximation to the anharmonic coupling between in-plane and out-of-plane acoustic modes in graphene provides additional theoretical reasons to show that the dispersion relation of the bending mode, $\omega_A(k)$, must be necessary linear at small wave numbers [9]. It is remarkable that the perturbation analysis of Amorim *et al.* [8] and the adiabatic approach of

*Corresponding author: ramirez@icmm.csic.es

Adamayan *et al.* [9], even though they differ in the anharmonic terms used to describe the phonon-phonon coupling, reach the same conclusion. Namely, the existence of a linear dispersion relation of the bending mode at small wave numbers. This term excludes, distinctively, the appearance of power-law divergences in the mean-square amplitude, $\langle h^2 \rangle$, of the out-of-plane thermal fluctuations as the area of the layer increases. The resulting amplitudes should then display a much slower logarithmic grow as a function of the number of atoms N [5,9].

Here, a series of classical molecular dynamics (MD) simulations of a free suspended graphene sheet are presented using the empirical long-range carbon bond order potential (LCBOPII) [10,11]. The focus lies on the characterization of the average height fluctuations under conditions of zero stress and temperatures up to 2000 K. Finite size effects have been considered by simulation of cells containing between 10^3 and 3×10^4 atoms. The analysis of the simulations is based upon an atomistic model, which has the distinct advantage over continuous models of providing information on both the acoustic and optical oscillations in the direction perpendicular to the layer. Particular emphasis is set upon the characterization of effects related to the anharmonicity of the employed interatomic potential. In this respect, an advantage of the numerical simulation over analytical approaches is that the full anharmonicity of the potential model is taken into account.

The structure of this paper is as follows. In Sec. II, we summarize the Fourier analysis of the symmetric and antisymmetric out-of-plane fluctuations. Basic equations are presented in Sec. II A, while a relation used to fit the k dependence of the acoustic height fluctuations is presented in Sec. II B. The analysis of the simulation results is given in Sec. III. The temperature dependence of the mean-square height fluctuations of the acoustic modes is studied in Sec. III A, while the related acoustic dispersion relation is the topic of Sec. III B. Anharmonic effects in the bending sound velocity, bending rigidity and frequencies of optical out-of-plane modes are studied in Sec. III C. The divergence of out-of-plane amplitudes with the system size is analyzed at 300 K in Sec. III D. A brief discussion of the results is presented in Sec. IV. Finally, we summarize our conclusions in Sec. V. Technical details concerning the MD simulations are given in Appendix A.

II. FOURIER ANALYSIS OF OUT-OF-PLANE FLUCTUATIONS

MD simulations were performed in both NVT and NPT ensembles (N being the number of atoms, V is the area of the simulation cell, P the trace of the 2D stress tensor divided by 2, and T the temperature). The simulation cell was defined by a supercell generated with a two-dimensional (2D) rectangular cell, $(\mathbf{a},\mathbf{b})$. For technical details concerning the simulation setup see Appendix A. Here we focus on the physics behind the Fourier analysis of out-of-plane modes.

A. Basic equations

The position of the jth atom of the simulation cell is represented by a vector

$$\mathbf{r_j} = (\mathbf{u_j}, z_j) \,, \tag{1}$$

where $\mathbf{u_j}$ is a 2D vector in the $(\mathbf{a},\mathbf{b})$ plane. The height of the atom is

$$h_j = z_j - \bar{z}, \tag{2}$$

with $\bar{z} = \sum_{j=1}^{N} z_j/N$ being the average height of the layer. The carbon atoms in graphene are divided into two sublattices, α and β, as shown in Appendix A. The discrete Fourier transform (dFT) of the heights of the carbon atoms in the sublattice α is

$$H_{\alpha,n} = \frac{2}{N} \sum_{j=1}^{N/2} h_j e^{-i\mathbf{k_n}\mathbf{u_j}} \,. \tag{3}$$

Here, the index j runs only over α atoms. The set of N_k vectors, $\mathbf{k_n}$, whose wavelengths are commensurate with the simulation cell, is defined in Appendix A. A similar expression defines $H_{\beta,n}$ as the dFT of the heights of the β sublattice. One can define the dFT of the symmetric and antisymmetric linear combinations of heights of α and β atoms:

$$A_n = \frac{H_{\alpha,n} + H_{\beta,n}}{2} \,, \tag{4}$$

$$O_n = \frac{H_{\alpha,n} - H_{\beta,n}}{2} \,. \tag{5}$$

At the Γ point, i.e., when $\mathbf{k_n} = \mathbf{0}$ in Eq. (3), the phase difference between two atoms (α and β) in a hexagonal unit cell is 0 (π) for the symmetric (antisymmetric) combination. However, for a generic $\mathbf{k_n}$ point, the phase difference is modulated by the value of the scalar product $\mathbf{k_n}\mathbf{u_j}$, which differs for α and β atoms. This phase modulation is similar to that encountered for the acoustic and optical modes of a lattice with a base of two atoms [12]. We will see later that, for the $\mathbf{k_n}$ points within the first hexagonal Brillouin zone (BZ), the module of the complex coefficients, $\bar{A}_n$ and $\bar{O}_n$, are estimators for the amplitude of the acoustic (ZA) and optical (ZO) vibrational modes of graphene with polarization vector along the z direction.

The ensemble average height fluctuation

$$\langle h^2 \rangle = \frac{1}{N} \left\langle \sum_{j=1}^{N} h_j^2 \right\rangle \tag{6}$$

is related to the set of spectral amplitudes $\langle \bar{A}_n^2 \rangle$ and $\langle \bar{O}_n^2 \rangle$ by the Parseval's theorem of the dFT in Eq. (3). Taking into account the definitions in Eqs. (4) and (5), one gets

$$\langle h^2 \rangle = \frac{2}{N} \left(\sum_{n=1}^{N_k} \langle \bar{A}_n^2 \rangle + \langle \bar{O}_n^2 \rangle \right) . \tag{7}$$

Then, within an atomistic description of graphene, the average height fluctuation is the sum of the symmetric and antisymmetric contributions. We will quantify later the relative contribution of both modes.

Another interest of the spectral amplitudes, $\langle \bar{A}_n^2 \rangle$ or $\langle \bar{O}_n^2 \rangle$, is their relationship to the vibrational frequencies of the corresponding vibrational modes. In the harmonic limit, one has

$$\rho \omega_{A,n}^2 = \frac{k_B T}{V_a \langle \bar{A}_n^2 \rangle} \,, \tag{8}$$

where k_B is the Boltzmann constant, $\rho = m/V_a$ is the atomic density of the layer, m is the atomic carbon mass, and

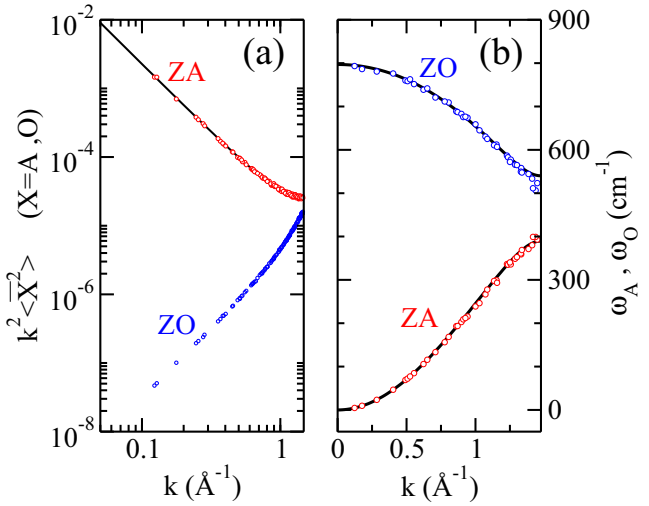

FIG. 1. (a) Log-log plot of the spectral amplitudes of the symmetric (acoustic, ZA) and antisymmetric (optical, ZO) modes of graphene derived from NPT simulations at 1 K. The $\mathbf{k_n}$ points, defined in Eq. (A5), correspond to a simulation cell with 960 atoms. The symbols show the square of the amplitude times k^2 as a function of module of the wave vector k. The continuous line is the least squares fit of the acoustic branch to Eq. (13). The largest displayed k point corresponds to the point M at the boundary of the hexagonal BZ ($k_M = 1.48$ Å^{-1}). (b) The dispersion relations of the ZA and ZO bands of graphene, as derived by Eq. (8), are shown by circles. The continuous lines are calculated by diagonalizing the dynamical matrix of the LCBOPII model along the ΓM direction of the hexagonal BZ.

$V_a = V/N$ the area per atom in the x,y plane. Although this relation between frequency and spatial amplitude is exact only in the harmonic limit, it has been applied in the context of anharmonic vibrations of molecules and solids as a reasonable linear response (LR) approximation [13,14]. Anharmonic shifts in the stretching frequency of hydrogen molecules adsorbed as isolated impurities in graphite and silicon were studied by this method [15,16]. Within this LR approximation anharmonic vibrational frequencies are estimated with Eq. (8) from *anharmonic vibrational amplitudes* that are obtained by computer simulations.

As illustration of the physical information of the spectral functions A_n and O_n, we have derived them in a classical NPT simulation of graphene with $N = 960$ atoms at $P = 0$ and $T = 1$ K. This temperature is chosen deliberately low with the purpose of having vibrational modes close to their harmonic limit. The simulation data can be then checked against analytical results.

In Fig. 1(a), the ensemble average of the dimensionless quantities $k_n^2\langle \bar{A}_n^2\rangle$ and $k_n^2\langle \bar{O}_n^2\rangle$ is shown as a function of the module of the wave vector, $k = |\mathbf{k}|$. The graphical representation as a function of k (instead of the vector $\mathbf{k}$) is justified by the in-plane isotropy of graphene. The isotropy is particularly valid in the elastic long-wavelength limit ($k \to 0$), although less true when the vector $\mathbf{k}$ approaches the boundary of the 2D hexagonal BZ [17]. As expected, the amplitudes for the symmetric branch are always larger that those of the asymmetric branch, and the difference increases in the long-wavelength limit.

The mean-square height $\langle h^2\rangle$ obtained in the NPT simulation at 1 K is $\langle h^2\rangle = 5.9 \times 10^{-4}$ Å^2. The contribution from the symmetric and antisymmetric modes derived by Eq. (7) amounts to 89% and 11%, respectively. Note that the contribution of the antisymmetric mode to the height fluctuation $\langle h^2\rangle$ is significant. However, to the best of our knowledge this contribution has never been quantified in previous simulations of graphene [5,7,18].

The wave numbers, ω_A and ω_O, derived by Eq. (8) from the amplitudes of the ZA and ZO modes are displayed as circles in Fig. 1(b). For comparison, the continuous lines show the frequencies obtained by diagonalizing the dynamical matrix of graphene along the Γ-M direction of the hexagonal BZ. The dynamical matrix was calculated with the same potential model (LCBOPII) as employed in the simulations. Vibrational frequencies of *both* acoustic and optical branches are reproduced accurately by the analysis of spectral amplitudes. It is remarkable that one gets realistic vibrational frequencies even near the boundary of the first hexagonal BZ. This one-to-one correspondence between symmetric (antisymmetric) out-of-plane fluctuations and acoustic (optical) vibrational amplitudes is somewhat lost when the vector $\mathbf{k_n}$ lies outside the first BZ. The spatial relation between the $\mathbf{k_n}$ grid and the hexagonal BZ is displayed in Fig. 8 in Appendix A. The relative large contribution (11%) of the asymmetric band to $\langle h^2\rangle$ is caused by the increasing acoustic character of the asymmetric out-of-plane fluctuations at k values larger than those shown in Fig. 1.

The realistic prediction of the ZA and ZO vibrational bands in Fig. 1(b) encourages us to apply this spectral analysis at higher temperatures, where anharmonic effects are expected to be relevant. However, an additional numerical tool would be helpful for the study of the long-wavelength limit of the acoustic modes. Namely, a realistic analytical function to fit the k dependence of its spectral amplitude.

B. Atomistic model for the acoustic spectral amplitudes

The phenomenological dispersion relation for the acoustic branch of a continuous membrane is

$$\rho\omega_A^2 = \sigma k^2 + \kappa k^4 , \tag{9}$$

where σ is the external stress, and κ is the bending rigidity. This relation could be used, with the help of Eq. (8), to fit the k dependence of the function $k_n^2\langle \bar{A}_n^2\rangle$ [see Fig. 1(a)]. However, the interval $[0,k_A]$, where the phenomenological expression is valid, is not clearly defined. Therefore it is convenient to work with an improved dispersion relation for graphene based on an atomistic model instead of a continuous limit as in Eq. (9).

The simplest atomic model that displays an acoustic flexural mode is a one-dimensional chain of atoms with interactions up to second nearest neighbors. The dispersion relation for this model has the following analytical form (see Appendix B)

$$\rho\omega_A^2 = D\left[\sin^2(Lk/2) - C\sin^2(Lk)\right] , \tag{10}$$

where D, L, and C are treated here as adjustable parameters. The Taylor expansion of this analytical function contains only even powers of k. The first two coefficients, as defined in

TABLE I. Parameters D, L, and C obtained from Eq. (13) by least squares fits of the simulated values of $k_n^2\langle\bar{A}_n^2\rangle$ at several temperatures. The fits were performed in the k interval defined by $k < 1$ Å^{-1}. V_a is the area per atom. The last columns are the linear term of the acoustic dispersion relation, σ, and the bending rigidity, κ. The results correspond to a simulation cell with 960 atoms.

T (K)	D (eV Å^{-4})	L (Å)	C	V_a (Å^2/atom)	σ (eV Å^{-2})	κ (eV)
1	4.716	1.491	0.2500	2.6189	0.000	1.49
50	3.320	1.645	0.2499	2.6185	0.001	1.52
300	2.904	1.727	0.2491	2.6173	0.008	1.61
1000	1.693	2.059	0.2480	2.6183	0.014	1.88
2000	1.292	2.280	0.2474	2.6279	0.018	2.15

Eq. (9), are

$$\sigma = DL^2\left(\frac{1}{4} - C\right), \tag{11}$$

$$\kappa = DL^4\left(\frac{C}{3} - \frac{1}{48}\right). \tag{12}$$

Following Eqs. (8) and (10), the simulated results of $k_n^2\langle\bar{A}_n^2\rangle$ will be fitted by a least squares method to the function

$$f(k) = \frac{k_B T}{V_a}\frac{k^2}{D\left[\sin^2(Lk/2) - C\sin^2(Lk)\right]}, \tag{13}$$

that depends on the parameters D,, and C. All the fits in this work were performed with k points satisfying $k < 1$ Å^{-1}.

The continuous line in Fig. 1(a) shows the fit of $k_n^2\langle\bar{A}_n^2\rangle$ for the simulation at 1 K. The fitted parameters are summarized in the first line of Table I. The value of the parameter $C = 1/4$ implies that $\sigma = 0$ here. A value of $\kappa = 1.49$ eV is derived from Eq. (12). We have checked that this value agrees, within the statistical error, with the numerical second derivative of ω_A:

$$\left(\frac{\kappa}{\rho}\right)^{1/2} = \frac{1}{2}\left(\frac{\partial^2\omega_A}{\partial k^2}\right)_{k=0}. \tag{14}$$

Here, ω_A was calculated by diagonalizing the dynamical matrix of the employed LCBOPII model. This ω_A band was shown by a continuous line in Fig. 1(b). The numerical second derivative at $k = 0$ gives the value $\kappa = 1.48$ eV.

III. SIMULATION RESULTS

NPT simulations of graphene were performed in the classical limit at external stress $P = 0$. Two cell sizes were employed to study temperatures in the range 50–2000 K. Predictions based on simulations with $N = 960$ atoms were checked against the results obtained with a larger cell with 8400 atoms.

A. Spectral amplitudes for ZA modes

The values of $k_n^2\langle\bar{A}_n^2\rangle$ for $N = 960$ are displayed as open circles in Fig. 2. The studied temperatures are 50, 300, 1000, and 2000 K. The size of the simulation cell implies that the shortest wave vector for the out-of-plane oscillations has $k = 0.12$ Å^{-1}. The largest displayed k corresponds to the point M

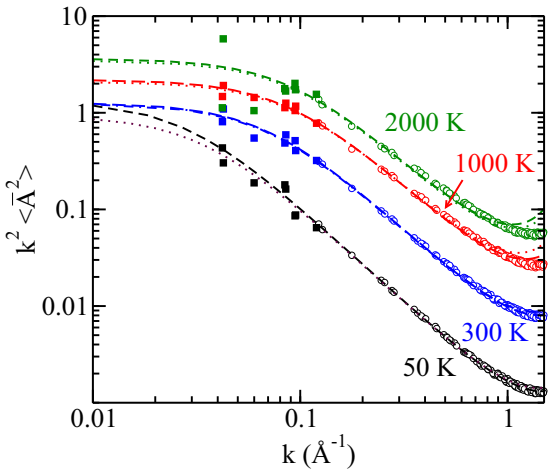

FIG. 2. Log-log plot of the spectral amplitudes of the ZA modes of graphene derived from NPT simulations at several temperatures. Open circles are results with $N = 960$ atoms for $k > 0.12$ Å^{-1}. Closed squares correspond to $N = 8400$ for $0.04 < k < 0.12$ Å^{-1}. The broken and dotted lines are least squares fits of the simulation results to Eq. (13). Broken lines are for $N = 960$ atoms and dotted ones for $N = 8400$. The broken and dotted lines at the same temperature are almost indistinguishable except at 50 K in the region of low k.

at the boundary of the hexagonal BZ. Least squares fits of the simulation data by Eq. (13) are shown by broken lines. The fitted coefficients D, L, and C are summarized in Table I. The fitted functions follow accurately the simulation data in the displayed k interval. Only at high temperature ($T \geqslant 1000$ K) there appears a small deviation between the fitted function and simulation data for $k > 1$ Å^{-1}.

In the region with $k < 0.12$ Å^{-1}, i.e., for long-wavelength oscillations, the fitted functions represent obviously an extrapolation of the simulation data. The extrapolation clearly predicts a flattening of the function $k^2\langle\bar{A}^2\rangle$ at the four studied temperatures. This flattening is absent in the harmonic limit displayed in Fig. 1(a). Numerically, C is the parameter that controls the behavior of the function $k^2\langle\bar{A}^2\rangle$ at low k. If the coefficient C becomes smaller than $1/4$ [see Eq. (11)], then the dispersion relation of the ZA modes displays a linear term, $\sigma > 0$. The fitted C coefficients in Table I decreases as the temperature increases. The value $\sigma > 0$ predicted by the simulations *at zero stress* is an anharmonic effect activated by the temperature.

As a consistency check for the extrapolated behavior of $k^2\langle\bar{A}^2\rangle$ at low k, the corresponding values for a larger cell with 8400 atoms are represented as closed squares in Fig. 2. To avoid an overcrowding of points, only those wave vectors with $k < 0.12$ Å^{-1} are plotted. The displayed squares correspond to oscillations with wavelengths ($\lambda = 2\pi/k$) that are inaccessible to the simulations with 960 atoms. The new points in the region $0.04 < k < 0.12$ Å^{-1} follow with reasonable accuracy the functions fitted with the smaller cell. This is true for the four studied temperatures. The simulation results of $k_n^2\langle\bar{A}_n^2\rangle$ with 8400 atoms have been also fitted with Eq. (13). The functions are plotted as dotted lines in Fig. 2. The dotted lines are nearly indistinguishable from the fits with the smaller cell (broken

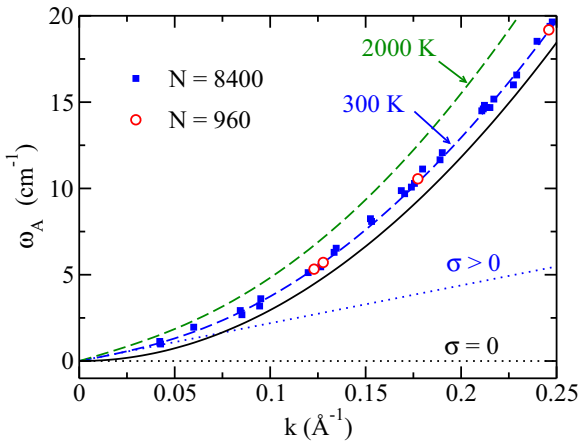

FIG. 3. Temperature dependence of the dispersion band of the ZA modes in the long-wavelength region. The continuous line is the classical $T \to 0$ limit, derived by diagonalizing the dynamic matrix along the ΓM direction. The broken lines correspond to Eq. (10) with the parameters D, L, and C obtained from the fits of $k_n^2\langle \bar{A}_n^2\rangle$ with 960 atoms at 300 and 2000 K, respectively (see Tab I). The open circles are the results derived from Eq. (8) with 960 atoms at 300 K. The closed squares are the corresponding results for 8400 atoms at 300 K. The straight dotted line with positive slope ($\sigma > 0$) is the linear term of the dispersion curve at 300 K. The slope is zero ($\sigma = 0$) for the quadratic dispersion in the limit $T \to 0$.

lines). A small difference at $k < 0.04$ Å^{-1} appears only at 50 K. We consider this agreement as a strong evidence that the dispersion relation in Eq. (10), which is the basic ingredient for the fit of the spectral amplitudes $k_n^2\langle \bar{A}_n^2\rangle$, provides a physically sound atomistic approximation for the out-of-plane acoustic oscillations of graphene.

B. Dispersion relation of ZA modes

The fitted constants D, L and C in Table I allow us to plot the acoustic dispersion relation, $\omega_A(k)$, according to Eq. (10). The curves at 300 and 2000 K are plotted as broken lines in Fig. 3. The dispersion relations are shown up to $k = 0.25$ Å^{-1}. For reference, we also display the harmonic $T \to 0$ limit derived by diagonalization of the dynamical matrix of the employed LCBOPII model, which was already plotted in Fig. 1(b). This limit, shown by a full line, displays a quadratic dispersion with vanishing linear term ($\sigma = 0$) as $k \to 0$. However, the dispersion curves at 300 and 2000 K show finite linear terms ($\sigma > 0$) as $k \to 0$. The dotted line with a positive slope displays the linear term at 300 K.

In Fig. 3, we have also plotted the discrete frequencies, $\omega_{A,n}$, derived from the spatial amplitudes $\langle \bar{A}_n^2\rangle$ by Eq. (8). The open circles are frequencies obtained from the simulation with 960 atoms. As expected, the open circles are in good agreement with the broken curve at 300 K, because both data were evaluated from the same set of $\langle \bar{A}_n^2\rangle$ values. However, the set of discrete frequencies derived from the simulation with 8400 atoms at 300 K provide an independent check of the results obtained with 960 atoms. These frequencies are plotted as closed squares in Fig. 3. The density of sampled k points is much larger than for 960 atoms. The closed squares are in reasonable agreement to the broken line predicted by the smaller cell at 300 K. It is remarkable that the dispersion relation, $\omega_A(k)$, displays a very small size effect, in the sense that a simulation with only 960 atoms seems to provide a reasonably converged result for this function.

The deviation of the dispersion curve at finite temperature from the harmonic $T \to 0$ limit is an anharmonic effect predicted by the simulation. Note that at the lowest k accessible in our simulations ($k = 0.04$ Å^{-1}, $\lambda = 150$ Å) the dispersion curve is very close to the straight line that plots its linear term. The estimated frequency for this k is only 1 cm^{-1} (3×10^{11} Hz) at 300 K, about two times larger than the harmonic $T \to 0$ limit. This anharmonic shift of the ω_A frequency is small in absolute value, but has a large effect for the out-of-plane carbon fluctuations. A related important anharmonic effect is that the sound velocity of the ZA branch, defined as

$$v_A = \left(\frac{\partial \omega_A}{\partial k}\right)_{k=0} = \left(\frac{\sigma}{\rho}\right)^{1/2}, \qquad (15)$$

becomes finite. At 300 K the sound velocity amounts to 0.4 km/s, while at 2000 K increases to 0.6 km/s. Our results are lower than the numerical estimations based on the adiabatic model of Adamyan *et al.,* which report a value of 1.1 km/s at 2000 K [9]. In the following section, we quantify the anharmonic effects of several important magnitudes related to the out-of-plane carbon fluctuations.

C. Anharmonic effect in σ, κ, and $\omega_O(\Gamma)$

The linear coefficient σ of the dispersion relation for ZA modes in graphene is displayed in Fig. 4(a). The results were obtained from NPT simulations at zero stress and temperatures between 1 and 2000 K. The coefficient σ increases from a vanishing value in the low-temperature (harmonic) limit to a value close to 0.02 eV Å^{-2} at 2000 K. The increase of σ seems to be linear at low temperatures. Above circa 700 K, σ grows less rapidly than linearly. A linear

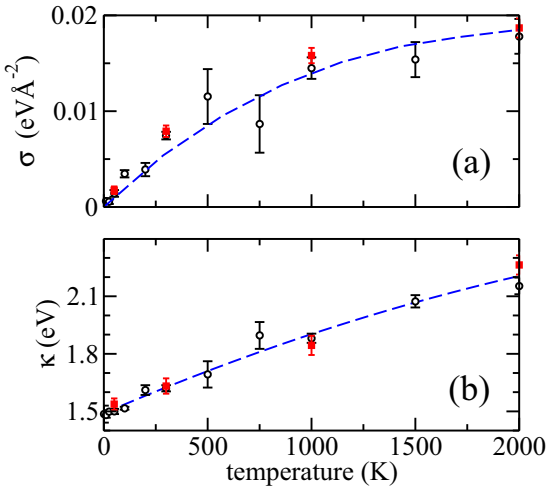

FIG. 4. (a) Temperature dependence of the linear coefficient, σ, of the dispersion relation of the ZA mode as derived from MD simulations up to 2000 K. (b) Bending rigidity κ of graphene as a function of temperature. Open circles were derived by a cell with 960 atoms, while filled squares correspond to a cell with 8400 atoms. The lines are guides to the eye.

dependence of σ with T was reported in a classical first-order perturbation treatment of graphene as a result of including anharmonic terms in the elastic model [8]. The adiabatic treatment of anharmonic effects of graphene in Ref. [9] was based on a quantum description of the out-of-plane vibrations. At temperatures above 700 K, they find that the oscillations behave classically and that σ should increase linearly with T, or even less than linearly when the temperature dependence of the in-plane elastic constants is taken into account. Our simulation results for σ are then in reasonable agreement to the expectations obtained by analytical treatments of anharmonic effects in the out-of-plane fluctuations of graphene [8,9].

The temperature dependence of the bending rigidity κ is displayed in Fig. 4(b). The plotted values were derived from the simulation results via Eq. (12). Starting from the harmonic $T \to 0$ limit of the employed LCBOPII model with $\kappa = 1.49$ eV, we observe that κ increases linearly with temperature. Above 700 K the increase becomes slightly slower than linear. At 2000 K, we get a bending rigidity $\kappa \approx 2.2$ eV. Previous atomistic simulations of graphene report contradicting results for the temperature dependence of the bending rigidity. Increase of κ with temperature has been reported in classical Monte Carlo simulations of graphene [19,20]. However, MD simulations between 200 and 1600 K were reported to present a decrease in κ from 1 eV to 0.4 eV [21]. Even a temperature independent κ has been suggested from MC simulations [22]. The determination of κ is usually performed by a best fit of simulated results of $\langle \bar{A}_n^2 \rangle$ in a k region where the slope can be approximated by the harmonic behavior of a continuous membrane [20,21]. However, the atomic character of graphene introduces uncertainty about the k region where the continuous membrane model is valid. Different results of κ may in part be caused from differences in the k range where the fit was performed.

The estimated temperature dependence of the ZO mode at the center of the BZ, $\omega_O(\Gamma)$, is displayed in Fig. 5. These values were derived from plots of ω_O as a function of k,

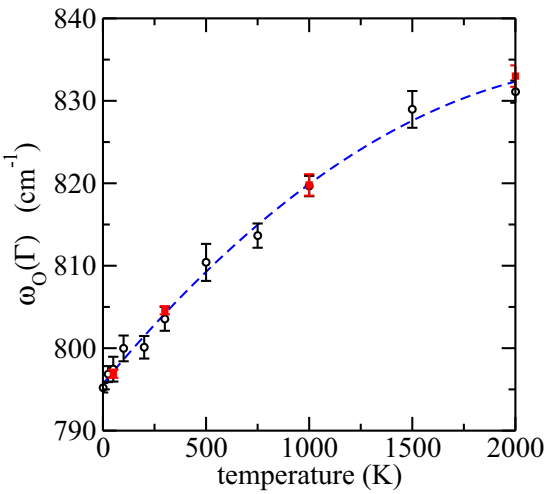

FIG. 5. Temperature dependence of the optical ZO mode at the center of the BZ. Open circles were derived from a cell with 960 atoms, while filled squares correspond to 8400 atoms. The line is a guide to the eye.

similar to that presented in Fig. 1(b) at 1 K. To extrapolate the frequency at Γ, i.e., at $k = 0$, we fitted a simple relation $\omega_O = A\cos(Lk)$ to the simulation results for $k < 0.6$ Å^{-1}. The anharmonicity of the employed model causes an increase of 4% in the frequency of the optical out-of-plane mode at Γ, when the temperature grows up to 2000 K. The linear increase at low temperatures slows down as the temperature increases, similarly to the behavior seen before for σ and κ. This dependence is a consequence of the increase of anharmonic effects as temperature grows. It is interesting that the effect of temperature in $\omega_O(\Gamma)$ is to make the vibrational mode harder. We are not aware of any previous prediction about the temperature dependence of $\omega_O(\Gamma)$ in graphene. This increase in vibrational frequency for rising temperature is similar to that found for acoustic modes with negative Grüneisen parameter in some solids [23].

D. Logarithmic divergence of mean-square heights with sample size

The mean-square height fluctuation $\langle h^2 \rangle$ of the carbon atoms is the sum of the contributions of symmetric, $\langle h_A^2 \rangle$ and antisymmetric modes $\langle h_O^2 \rangle$. From Eq. (7), one has

$$\langle h_A^2 \rangle = \frac{2}{N} \sum_{n=1}^{N_k} \langle \bar{A}_n^2 \rangle , \tag{16}$$

and a similar relation for $\langle h_O^2 \rangle$. We will use an analytical harmonic expression for $\langle h_A^2 \rangle$ and a simple estimation of $\langle h_O^2 \rangle$ to rationalize the size dependence of $\langle h^2 \rangle$ found in NPT simulations at 300 K with cell sizes up to 33 600 atoms.

For the asymmetric mode, we make a rough estimate

$$\langle h_O^2 \rangle \approx 0.16 \langle h_A^2 \rangle . \tag{17}$$

This relation is derived from our simulation results with 960 and 8400 atoms at 300 K. We find a ratio $\langle h_O^2 \rangle = 0.14 \langle h_A^2 \rangle$ for $N = 960$ atoms, while the factor becomes 0.18 for $N = 8400$ atoms. For the sake of simplicity, we have approximated $\langle h_O^2 \rangle$ for $N < 33\,600$ as the average of both results.

The analytical harmonic prediction for $\langle h_A^2 \rangle$ has been derived in Ref. [5] under the assumption that the dispersion relation for the acoustic mode, ω_A, is given by Eq. (9). The parameters σ and κ of the harmonic model will be taken from our simulation results with 960 atoms (see Table I).

Firstly, let us consider the hypothetical case where ω_A has a vanishing linear term (i.e., $\sigma = 0$ and therefore $\rho\omega_A^2 = \kappa k^4$). The harmonic limit of the mean-square fluctuations is [5]

$$\langle h_{A1}^2 \rangle = \frac{k_B T V_a N}{16\pi^4 \kappa} \sum_{j,l=-n}^{n}{}' \left(j^2 + l^2\right)^{-2} . \tag{18}$$

The sum is over a discrete k point mesh assuming a squared-shaped membrane with periodic boundary conditions. n is defined as the number of atoms along each direction of the plane, i.e., $n^2 = N$. The prime indicates that the term $j = l = 0$ is not included in the sum. $\langle h_{A1}^2 \rangle$ was calculated at 300 K as a function of N with the data for V_a and κ from Table I. The total mean-square height is then approximated under consideration of Eq. (17) as

$$\langle h_1^2 \rangle = 1.16 \langle h_{A1}^2 \rangle . \tag{19}$$

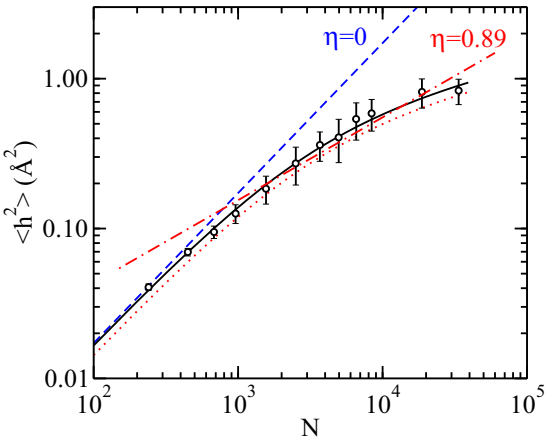

FIG. 6. Log-log plot of the mean-square fluctuation of out-of-plane modes of graphene as a function of the number of atoms in the simulation cell. Open symbols are results of NPT simulations at zero stress and $T = 300$ K. The dashed line displays the harmonic results for $\kappa = 1.61$ eV and $\sigma = 0$, while the continuous line represents the harmonic limit when $\sigma = 0.008$ eV/Å^{-1}. The curves include contributions from both the symmetric and antisymmetric modes. The dotted line is derived from the continuous one by subtraction of the antisymmetric mode contribution. The dash-dotted line is a power-law fit, $\langle h^2\rangle = cN^{1-(\eta/2)}$, of the simulation results for $N > 500$.

The result as a function of N is displayed in Fig. 6 by a dashed line. The expectation values, $\langle h^2\rangle$, obtained from NPT simulations using Eq. (6) for cell sizes up to 33 600 atoms are given by symbols. We note that Eq. (19) overestimates the out-of-plane height fluctuations by an unrealistic large amount.

Secondly, let us include the linear term of our simulations ($\sigma = 0.008$ eV Å^{-2} at 300 K) in the dispersion relation of Eq. (9). In this case, the harmonic limit of the mean-square height fluctuations becomes [5]

$$\langle h_{A2}^2\rangle = \frac{k_B T V_a N}{16\pi^4\kappa} \sum_{j,l=-n}^{n}{}' \left(j^2+l^2\right)^{-2} \times \left(1+\frac{\sigma V_a N}{4\pi^2\kappa}\left(j^2+l^2\right)^{-2}\right)^{-1}. \quad (20)$$

The result for the total height fluctuation,

$$\langle h_2^2\rangle = 1.16\langle h_{A2}^2\rangle, \quad (21)$$

is displayed in Fig. 6 by a full line. The harmonic model, with the finite sound velocity corresponding to our value of σ at 300 K, gives now a realistic description of the simulation results.

The dotted line in Fig. 6 is the symmetric contribution $\langle h_{A2}^2\rangle$ to the total mean-square fluctuation. Note that the explicit consideration of the antisymmetric mode improves the agreement between simulation results of $\langle h^2\rangle$ and the analytical model.

The harmonic approximations, $\langle h_{A1}^2\rangle$ and $\langle h_{A2}^2\rangle$, have different asymptotic behavior in the limit of large sample size. The summations in Eqs. (18) and (20) can be converted to integrals in a continuum approximation. The details are given elsewhere [5]. Here it suffices to quote that in a continuum limit

$$\langle h_{A1}^2\rangle \approx \frac{k_B T V_a N}{16\pi^3\kappa}, \quad (22)$$

$$\langle h_{A2}^2\rangle \approx \frac{k_B T}{4\pi\sigma} \ln\left(1+\frac{\sigma V_a N}{4\pi^2\kappa}\right). \quad (23)$$

Thus a finite value of σ reduces the divergence of the harmonic mean-square amplitude, which results in a proportionality to N in $\langle h_{A1}^2\rangle$, but diverges only logarithmically with N in $\langle h_{A2}^2\rangle$. The results of Fig. 6 show that our NPT simulations at zero stress are in reasonable agreement with a logarithmic divergence in the long-wavelength behavior of $\langle h^2\rangle$ with the number of atoms N. The essential ingredient for this agreement is the appearance of a linear term, $v_A k$, in the dispersion relation of ω_A. This term implies a finite sound velocity for the long-wavelength limit of the acoustic ZA modes.

TABLE II. Dispersion relation for ZA modes used in the interpretation of out-of-plane amplitudes of graphene. k interval gives regions where the model was applied in simulations. The next column summarizes the large size limit of the mean-square fluctuations.

$\rho\omega_A^2$	k interval (Å^{-1})	$\langle h_A^2\rangle$ ($N\to\infty$)	References
κk^4	[0.3,1] [7], [0.3,0.4] [34]	N	[7,21,34]
$\kappa_r k^{4-\eta}$	[0,0.2] [7], [0.4,1] [22]	$N^{1-(\eta/2)}$	[5,7,22]
Eq. (10)	[0,1]	$\ln N$	This work

IV. DISCUSSION

Best fits presented in the literature of simulated values of mean-square fluctuations, $\langle \bar{A}_n^2\rangle$ or $\langle h^2\rangle$, should be taken with caution. There is no general agreement about the theoretically best fitting model. Given that Eq. (8) defines a one-to-one correspondence between the amplitudes $\langle \bar{A}_n^2\rangle$ and the frequencies of ZA modes, one can distinguish the models just by the underlying dispersion relation.

Different dispersion relations used for graphene are summarized in Table II. Each model reproduces with reasonable accuracy simulation results in certain k regions. We consider that the apparent success of fitting simulation data to different models is due to the fact that information derived from the simulations is always partial. In particular, the long wavelength limit ($k\to 0$) is not easily accessible as the simulation time grows prohibitively with the cell size ($N\to\infty$) and also as the statistics of very low frequency modes worsens because of limited simulation time.

A further matter of concern is the function to be fitted. Both the absolute value of the function and the density of k points affect the result of the least squares method. In the present work we fitted the function $k_n^2\langle \bar{A}_n^2\rangle$. The reason is that for a flexural mode with a quadratic dispersion the value of $\langle \bar{A}_n^2\rangle$ decreases as k^{-4}, while the density of sampled points in k space increases as k^2, i.e., as the area of circular sectors of radius k. Thus for $k_n^2\langle \bar{A}_n^2\rangle$, the value of the fitted function times the density of sampled points becomes approximately independent of k. Evenly distributed weights in k space is a convenient feature for the least squares method. Let us present a specific example: if one performs the least squares fit with

the reciprocal function $(k_n\langle \bar{A}_n{}^2\rangle)^{-1}$, instead of $k_n^2\langle \bar{A}_n^2\rangle$, then the k_n points with a larger module will effectively have a larger weight in the fit. The reason is that both the value of the reciprocal function and the density of points increase now as k^2. As a consequence, the coefficient σ, derived from the best fit of the reciprocal function, is about two times larger than those presented in Table I.

One important physical difference between the three models in Table II is that a finite sound velocity for the acoustic out-of-plane vibrations, v_A, is predicted only by the model used in the present work. The other two dispersion relations in Table II imply that $v_A = 0$ at all temperatures. In this respect, our simulation results have received an independent confirmation from a recent theoretical paper that predicts, in terms of a clear physical picture, the acoustic-type dispersion of the bending mode [9]. The origin of the bending sound velocity is related to the *anharmonic* interaction between in-plane and out-of-plane vibrations due to nonlinear components in the strain tensor. The investigation by Adamyan *et al.* shows that the dispersion of the bending mode must be necessarily linear at small wave numbers [9]. We consider this behavior as an important physical property of graphene that is confirmed by our analysis of the NPT simulations.

Interestingly, a previous prediction of a linear component in the dispersion of the ZA mode was presented by Kumar *et al.* [24] based on electronic structure density functional theory calculations. In this work, the origin of the rigidity was traced to the coupling between vibrational and electronic degrees of freedom, arising from a curvature induced overlap between π orbitals in graphene [24]. The same result was suggested by Falkovsky [25] by the study of the symmetry constraints of the phonon dispersion curves of graphene. The bending velocity could be zero only if a definite condition is fulfilled for the force constants of the graphene lattice. The same fact was found for a one-dimensional atomic chain (see Appendix B). Using the value of force constants obtained by fitting experimental data of graphite he concluded that graphene possesses a small but finite bending stiffness [25].

Previous classical simulations of out-of-plane fluctuations of graphene have been analyzed in terms of a power-law behavior of $\langle h^2\rangle$ with a roughness exponent close to one, in agreement to the classical self-consistent calculation by Nelson and Peliti [6]. One may wonder what makes our classical simulations to deviate from this picture. In fact, by fitting our simulated values of $\langle h^2\rangle$ to a power law in Fig. 6, we get a roughness exponent $\eta = 0.89$ (dash-dotted line), close to the values reported in the literature [5,7]. We note that the set of cell sizes considered in our simulations is larger than in previous studies, which used only between three and six different cell sizes [5,7]. The whole range of studied cell sizes shows that the analytical model for $\langle h^2\rangle$ in Eq. (20) represents an improved agreement to the simulation results, in comparison to a power-law fit. We stress that the continuous line in Fig. 6 is not a fit, but an analytical model defined with plain physical quantities (σ and κ) derived from the symmetric out-of-plane fluctuations of our simulations.

The appearance of a finite bending sound velocity, v_A, translates into a roughness exponent $\eta = 2$. This is the roughness exponent obtained by Amorim *et al.* [8] in a quantum self-consistent perturbative calculation of anharmonic graphene. It may appear surprising that here the result of our classical simulations agrees with the roughness exponent of a quantum calculation ($\eta = 2$) but disagrees with the self-consistent classical perturbative result ($\eta = 1$). However, one should consider that the classical simulations include (numerically) the whole anharmonicity of the employed model potential. Therefore the disagreement of the classical simulation with the expectation of a classical first-order perturbation theory must not be necessarily considered as a kind of inconsistence. We expect to clarify this issue in a future work by including quantum effects in our simulations by the path integral formalism.

The analysis of the simulated trajectories of graphene, in particular the study of the asymmetric out-of-plane modes, allowed us the characterization of the optical bending branch of graphene. This analysis offers additional physical information that has not been previously considered in simulation studies of graphene.

V. CONCLUSIONS

We have presented a series of NPT simulations of graphene under zero stress conditions. The simulations included temperatures up to 2000 K and several cell sizes up to 33 600 atoms. The simulations were performed in the classical limit using the empirical LCBOPII model. The focus of this study has been the characterization of anharmonic effects associated to the out-of-plane oscillations of the layer. The symmetry of the lattice, with two atoms as a basis, imposes the presence of an acoustic and an optical branch for the out-of-plane oscillations. We have focused on an atomistic description of both out-of-plane modes. This description is more general than a continuous limit of the solid membrane, where optical out-of-plane modes are absent.

The mean-square out-of-plane fluctuations of carbon atoms have been analyzed with a model for the dispersion relation of the acoustic bending branch. The result of this analysis is the characterization of several anharmonic effects as a function of temperature. The most important finding is that the mean-square out-of-plane fluctuation of carbon is compatible with the presence of a linear dispersion term in the acoustic ZA branch at low wave numbers. This effect is a consequence of the anharmonicity of the interatomic potential and therefore increases with temperature as the amplitude of atomic vibrations increases. The bending sound velocity, derived from the linear dispersion term of the ZA mode, increases from 0 to 0.6 km/s when the temperature rises from the zero temperature limit to 2000 K. At the same time, the bending rigidity of graphene is found to increase in this temperature window from 1.49 to 2.2 eV. The frequency of the optical ZO modes at the Γ point of the Brillouin zone displays a shift of 4% as temperature increases up to 2000 K. The hardening of these modes with temperature is again a consequence of the anharmonicity of the model.

The existence of a finite bending velocity in graphene implies that the amplitude of the out-of-plane fluctuations, $\langle h^2\rangle$, is strongly reduced in the long-wavelength limit. If the dispersion relation of the ZA branch were strictly quadratic, $\langle h^2\rangle$ would diverge proportional to the number of atoms N of the layer. A finite sound velocity implies that the divergence in $\langle h^2\rangle$

is reduced becoming proportional to $\ln N$. The results of our simulations are consistent with recent analytical findings [8,9].

ACKNOWLEDGMENTS

This work was supported by Dirección General de Investigación, MINECO (Spain) through Grant Nos. FIS2012-31713, FIS2013-47350, and FIS2015-64222-C2-1-P. The authors benefited from the kind support of J. H. Los in the implementation of the LCBOPII potential. We thank R. Roldán fora critical reading of the manuscript.

APPENDIX A: COMPUTATIONAL CONDITIONS

The classical MD simulations of graphene were performed on supercells generated with a two-dimensional (2D) rectangular cell. The relation of the rectangular axes $(\mathbf{a},\mathbf{b})$ to the standard hexagonal cell $(\mathbf{a}_h,\mathbf{b}_h)$ is shown in Fig. 7. The simulation cell is described by a 2×2 matrix G whose columns are the Cartesian coordinates of the cell vectors

$$G = (L_x\mathbf{a}, L_y\mathbf{b}) \,, \tag{A1}$$

where L_x and L_y are positive integers. The supercell (L_x,L_y) is chosen to have similar linear dimension in the x and y directions. We have performed simulation on supercells of several sizes having between 960 and 33 600 atoms. Periodic boundary conditions were applied to the 2D simulation cell. The area of the simulation cell is $V = |G|$. It is important to note that the graphene lattice is constructed with a base of two atoms (α and β), which are distinguished in Fig. 7 as open and closed circles, respectively. In the ideal lattice, each β atom is related to an α atom by a fixed vector

$$\mathbf{u}_{\beta,j} = \mathbf{u}_{\alpha,j} + \frac{\mathbf{b}}{3} \,. \tag{A2}$$

The potential energy U of graphene has been obtained with the LCBOPII model [10,11]. A slight modification of the original torsion parameters was made in order to increase the bending constant of a flat layer in the zero temperature limit from $\kappa = 1.1$ eV to $\kappa = 1.48$ eV [26]. The latter value is in better agreement to *ab initio* electronic structure calculations with values of κ in a range from 1.46 to 1.6 eV [27]. The temperature was controlled by chains of four Nosé-Hoover thermostats coupled to each of the Cartesian atomic coordinates. In the case of the NPT ensemble, an additional chain of four barostats was coupled to the volume [28]. To integrate the equations of motion, a reversible reference system propagator algorithm (RESPA) was employed [29]. For the evolution of thermostats and barostats, a time step $\delta t = \Delta t/4$ was used, where Δt is the time step associated to the calculation of forces. A value of $\Delta t = 1$ fs was found to provide adequate convergence, although some check simulations at 1000 K were performed with a smaller time step of 0.5 fs. Atomic forces were derived analytically by the derivatives of the potential energy U. The stress tensor estimator was similar to that used in a previous work [30]:

$$\sigma_{xy} = \left\langle \frac{1}{V}\left(\sum_{i=1}^{N} m v_{ix} v_{iy} - \frac{\partial U}{\partial \epsilon_{xy}}\right)\right\rangle , \tag{A3}$$

where v_{ix} is a velocity coordinate, ϵ_{xy} is a component of the 2D strain tensor, and the brackets $\langle\cdots\rangle$ indicates an ensemble average. The derivative of U with respect the strain tensor was performed analytically. Typical runs consisted of 5×10^5 MD steps (MDS) for equilibration, followed by runs using between 2×10^6 and 8×10^6 MDS for calculation of equilibrium properties. Both isotropic and full cell fluctuations were programed for the NPT ensemble. The structural analysis was performed on subsets of 8×10^3 configurations stored at equidistant times during the whole simulation run. Error bars were evaluated by dividing the total simulation run into four blocks and by calculating the standard deviation of the block averages.

The reciprocal lattice corresponding to the simulation cell is defined by the matrix

$$G_r = 2\pi\left(G^{-1}\right)^T \,. \tag{A4}$$

The columns of this matrix $(\mathbf{a}^*,\mathbf{b}^*)$ define the wave vectors $\mathbf{k}_n$ whose wavelengths are commensurate with the simulation cell

$$\mathbf{k}_n = n_x\mathbf{a}^* + n_y\mathbf{b}^* \,, \tag{A5}$$

with $n_x = 0,\ldots,L_x-1$ and $n_y = 0,\ldots,L_y-1$. The total number of $\mathbf{k}_n$ points is $N_k = L_xL_y$. The $\mathbf{k_n}$ grid used in the Fourier transform of heights of the carbon atoms in a (20,12) supercell is displayed in Fig. 8.

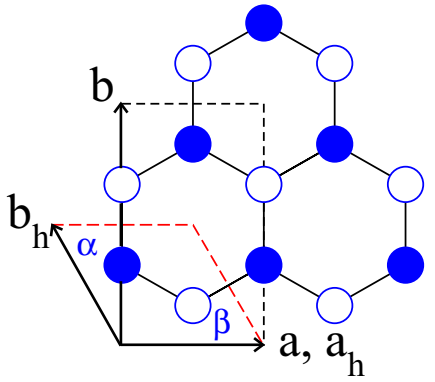

FIG. 7. The rectangular cell $(\mathbf{a},\mathbf{b})$ used in the simulations is displayed together with the standard hexagonal cell $(\mathbf{a}_h,\mathbf{b}_h)$ of the graphene lattice. The atomic base of the lattice is made up of two atoms, labeled as α (full circles) and β (open circles).

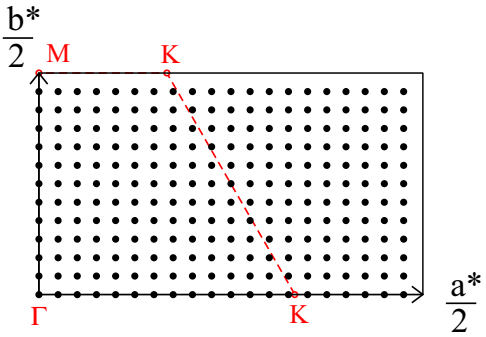

FIG. 8. Reciprocal cell $(\mathbf{a}^*,\mathbf{b}^*)$ of the rectangular axes $(\mathbf{a},\mathbf{b})$ employed in the simulations. Γ, M, and K label the special positions of the 2D hexagonal BZ. The filled dots represent the $\mathbf{k_n}$ grid used in the Fourier transform of atom heights for a (20,12) supercell with 960 atoms.

APPENDIX B: DISPERSION RELATION FOR A LINEAR CHAIN

The dispersion relation $\omega(k)$ for a linear chain of atoms with elastic interactions up to second nearest neighbors is a a simple extension of the textbook solution for a first nearest-neighbors interaction [31]. The interest of this extension is that depending on the relation between the two force constants (c_1 and c_2), one finds three types of elastic behavior similar to those of a graphene sheet in the harmonic limit [32,33].

Let us consider the atoms along the x axis at coordinates $x_s = sL$, with L being the interatomic distance, and s an integer that enumerates the atoms. The height of the sth atom with respect to the axis is h_s and the k points are defined in the interval $[-\pi/L,\pi/L]$. Considering the collective mode of amplitude A

$$h_s = Ae^{-ix_sk}e^{-i\omega t} , \tag{B1}$$

the equation of motion of for the s'th atom with mass m is

$$m\frac{\partial^2 h_s}{\partial t^2} = c_1(h_{s+1} - h_s) + c_1(h_{s-1} - h_s) + c_2(h_{s+2} - h_s) + c_2(h_{s-2} - h_s) . \tag{B2}$$

Performing the time derivative and taking into account that $h_{s+n} = h_s e^{-inLk}$, one gets after dividing by h_s,

$$-m\omega^2 = c_1(e^{-iLk} + e^{iLk} - 2) + c_2(e^{-i2Lk} + e^{i2Lk} - 2) . \tag{B3}$$

The sum of the complex exponentials gives a cosine function that is simplified by the trigonometric relation $1 - \cos k = 2\sin^2(k/2)$ with the result

$$\rho\omega^2 = D\left[\sin^2\left(\frac{Lk}{2}\right) - C\sin^2(Lk)\right] , \tag{B4}$$

with the constants $D = 4c_1/L$ and $C = -c_2/c_1$. The atomic density is $\rho = m/L$. Depending on the value of C, there appear three different elastic behaviors: (a) if $C < 1/4$, the dispersion relation is linear in the long-wavelength limit, $\rho\omega^2 = \sigma k^2$ with $\sigma = L(c_1 + 4c_2)$; (b) if $C = 1/4$, the dispersion relation is quadratic for long-wavelength oscillations, $\rho\omega^2 = \kappa k^4$, with $\kappa = c_1L^3/4$; (c) if $C > 1/4$, the linear system is unstable ($\omega^2 < 0$) for $k < (\sigma/\kappa)^{1/2}$.

[1] J. C. Meyer, A. K. Geim, M. I. Katsnelson, K. S. Novoselov, T. J. Booth, and S. Roth, Nature (London) **446**, 60 (2007).
[2] R. Thompson-Flagg, M. Moura, and M. Marder, Europhys. Lett. **85**, 46002 (2009).
[3] B. Amorim, A. Cortijo, F. de Juan, A. Grushin, F. Guinea, A. Gutiérrez-Rubio, H. Ochoa, V. Parente, R. Roldán, P. San-Jose, *et al.*, Phys. Rep. **617**, 1 (2016).
[4] D. A. Kirilenko, A. T. Dideykin, and G. Van Tendeloo, Phys. Rev. B **84**, 235417 (2011).
[5] W. Gao and R. Huang, J. Mech. Phys. Solids **66**, 42 (2014).
[6] D. Nelson and L. Peliti, J. Phys. **48**, 1085 (1987).
[7] J. H. Los, M. I. Katsnelson, O. V. Yazyev, K. V. Zakharchenko, and A. Fasolino, Phys. Rev. B **80**, 121405 (2009).
[8] B. Amorim, R. Roldán, E. Cappelluti, A. Fasolino, F. Guinea, and M. I. Katsnelson, Phys. Rev. B **89**, 224307 (2014).
[9] V. M. Adamyan, V. N. Bondarev, and V. V. Zavalniuk, arXiv:1510.07878.
[10] J. H. Los and A. Fasolino, Phys. Rev. B **68**, 024107 (2003).
[11] J. H. Los, L. M. Ghiringhelli, E. J. Meijer, and A. Fasolino, Phys. Rev. B **72**, 214102 (2005).
[12] N. W. Ashcroft and D. N. Mermin, *Solid State Physics* (Saunders College, Philadelphia, 1976).
[13] R. Ramírez and T. López-Ciudad, J. Chem. Phys. **115**, 103 (2001).
[14] R. Ramírez and C. P. Herrero, Phys. Rev. B **72**, 024303 (2005).
[15] C. P. Herrero and R. Ramírez, Phys. Rev. B **80**, 035207 (2009).
[16] C. P. Herrero and R. Ramírez, Phys. Rev. B **82**, 174117 (2010).
[17] P. Lambin, Appl. Sci. **4**, 282 (2014).
[18] R. Roldán, A. Fasolino, K. V. Zakharchenko, and M. I. Katsnelson, Phys. Rev. B **83**, 174104 (2011).
[19] S. Costamagna, M. Neek-Amal, J. H. Los, and F. M. Peeters, Phys. Rev. B **86**, 041408 (2012).
[20] K. V. Zakharchenko, J. H. Los, M. I. Katsnelson, and A. Fasolino, Phys. Rev. B **81**, 235439 (2010).
[21] P. Liu and Y. W. Zhang, Appl. Phys. Lett. **94**, 231912 (2009).
[22] A. Lajevardipour, M. Neek-Amal, and F. M. Peeters, J. Phys.: Condens. Matter **24**, 175303 (2012).
[23] N. Mounet and N. Marzari, Phys. Rev. B **71**, 205214 (2005).
[24] S. Kumar, K. P. S. S. Hembram, and U. V. Waghmare, Phys. Rev. B **82**, 115411 (2010).
[25] L. Falkovsky, Phys. Lett. A **372**, 5189 (2008).
[26] J. H. Los (private communication).
[27] A. Politano, A. R. Marino, D. Campi, D. Farías, R. Miranda, and G. Chiarello, Carbon **50**, 4903 (2012).
[28] M. E. Tuckerman and A. Hughes, in *Classical & Quantum Dynamics in Condensed Phase Simulations*, edited by B. J. Berne and D. F. Coker (Word Scientific, Singapore, 1998), p. 311.
[29] G. J. Martyna, M. E. Tuckerman, D. J. Tobias, and M. L. Klein, Mol. Phys. **87**, 1117 (1996).
[30] R. Ramírez, C. P. Herrero, E. R. Hernández, and M. Cardona, Phys. Rev. B **77**, 045210 (2008).
[31] C. Kittel, *Introduction to Solid State Physics* (Wiley, New York, 1966).
[32] P. L. de Andres, F. Guinea, and M. I. Katsnelson, Phys. Rev. B **86**, 144103 (2012).
[33] P. L. de Andres, F. Guinea, and M. I. Katsnelson, Phys. Rev. B **86**, 245409 (2012).
[34] D. A. Kirilenko, Tech. Phys. Lett. **39**, 325 (2013).